IEEE Access
Multidisciplinary ⋮ Rapid Review ⋮ Open Access Journal

Received December 14, 2018, accepted January 6, 2019, date of publication January 11, 2019, date of current version February 4, 2019.

*Digital Object Identifier 10.1109/ACCESS.2019.2892505*

# Ground-Based Radar Detection for High-Speed Maneuvering Target via Fast Discrete Chirp-Fourier Transform

**XIANG HUANG[1], SHIYANG TANG[1], (Member, IEEE), LINRANG ZHANG[1], AND SHENGYUAN LI[2]**
[1]National Laboratory of Radar Signal Processing, Xidian University, Xi'an 710071, China
[2]China Academy of Space Technology, Xi'an 710071, China

Corresponding author: Shiyang Tang (sytang@xidian.edu.cn)

This work was supported in part by the National Natural Science Foundation of China under Grant 61601343, Grant 61731023, and Grant 61671361, in part by the China Postdoctoral Science Foundation Funded Project under Grant 2016M600768, and in part by the National Natural Science Foundation of the Shaanxi Province under Grant 2018JM6054.

**ABSTRACT** Detection of high-speed maneuvering targets has attracted a great deal of attention recently. There are two main problems to be solved: improving detection ability under the condition of complicated range migration and Doppler frequency migration effects, and reducing computational load. Different from most existing fast algorithms which are at the cost of detection ability, this paper devises a computationally attractive method with excellent detection performance. First, the keystone transform is carried out to remove linear range migration. Thereafter, a fast discrete chirp-Fourier transform (FDCFT) based on radix-4 decomposition is proposed to compensate the undersampled linear Doppler frequency migration and quadratic Doppler frequency migration. Because of exploiting inherent symmetry and periodicity as in the fast Fourier transform (FFT), the FDCFT can largely reduce the computational complexity without performance loss. The novelty of the proposed algorithm lies in combining linear transform with the concept of decimation-in-time FFT, which avoids the demanding multi-dimensional search and severe performance loss via introducing nonlinear transforms. It is shown that the proposed method has an approximately optimal detection performance but with relatively low computational cost.

**INDEX TERMS** Fast discrete chirp-Fourier transform, Doppler frequency migration, high-speed maneuvering target, coherent integration.

## I. INTRODUCTION

With the development of stealth and supersonic technology, modern aerial targets have presented the characteristics of high speed, strong maneuverability, long range, and low radar cross section (RCS). The traditional moving target detection algorithm has no enough capacity to detect these high speed maneuvering targets, and new detection algorithms are receiving significant research efforts [1]–[3]. The long-time integration technique is considered effective to improve the ultimate target detection performance [4], [5]. Generally, the long-time integration can be divided into coherent integration and incoherent integration [6]. Because of compensating phase fluctuation among different pulses, the coherent integration method could obtain better integration performance than that of the incoherent integration one. However, the high speed will result in range migration (RM) and velocity ambiguity for low pulse repetition frequency radar. Moreover, the strong maneuverability will lead to complex Doppler frequency migration (DFM) during the coherent integration time [7]–[10]. The detection performance would suffer from great loss if the RM and DFM cannot be compensated in a proper way.

Typical detection algorithms, such as Keystone transform (KT) [11]–[13], Radon Fourier transform (RFT) [4], [14], [15], and frequency-domain deramp-keystone transform (FDDKT) [16] have been proposed to compensate linear RM and realize coherent integration for high-speed target. However, they suffer from integration performance loss without considering the effects of DFM induced by the target's complex motions. The KT-Dechirp method [17], scaling processing and fractional Fourier transform (SPFRFT) [18], improved axis rotation (IAR) based methods [19], [20], RFT-KT [21], Radon-FRFT (RFRFT) [22] and Radon-Lv's distribution (RLVD) [23] have been presented to eliminate

RM and DFM, and can achieve coherent accumulation for maneuvering targets in the uniform acceleration scene. Recently, Sun *et al*. [24] have presented a fast detection method based on KT and matched filtering process (MFP) to obtain an excellent integration and detection performance. Nevertheless, these methods only consider the compensation of DFM induced by the target's radial acceleration. As for the target with strong maneuverability, the radial jerk cannot be ignored, especially when the coherent integration time is long enough to bring about serious DFM [5], [25].

In order to detect the maneuvering target with a jerk, Chen *et al*. [26] have proposed the Radon-linear canonical ambiguity function (RLCAF) and Radon-fractional ambiguity function (RFRAF) [27], which combines dimensionality reduction and motion parameter search to realize the simultaneous compensation of complex RM and DFM. However, these methods have weak detection ability in low signal-to-noise ratio (SNR), and huge computational load due to multi-dimensional parameter search. In order to further improve detection ability, improved axis rotation and discrete chirp Fourier transform (DCFT) (IAR-DCFT) [28] is utilized to correct the RM via IAR and compensate the complex DFM effects by DCFT. However, the search step length of axis rotation angle changes nonlinearly with that of velocity, which may result in serious parameter estimation errors and limit its applicability in high speed scene. In [29], the generalized Radon Fourier transform (GRFT) is presented to realize long time coherent integration for the arbitrary parameterized motion model under low SNR condition. In [30], we have proposed a method based on Radon-advanced discrete chirp Fourier transform (RADCFT) to detect low-observable maneuvering target. Nevertheless, these two methods are both computationally prohibitive because of 4-D search of range, velocity, acceleration, and jerk. To reduce the computational load, fast methods based on time-frequency analysis algorithms are proposed, such as KT and cubic phase function (KT-CPF) [31], second-order KT and modified integrated cubic phase function (SKT-MICPF) [32], KT and coherently integrated cubic phase function (KT-CICPF) [33], and SKT and generalized Hough-HAF transform (SKT-GHHAF) [10]. Since the CPF, Hough, and HAF are all nonlinear transforms, these fast methods suffer from severe performance loss compared with linear transforms, and thus may be limited in the extremely low SNR condition. There are also fast detection methods based on reduced-order principle, such as adjacent cross correlation function (ACCF) [25] and time reversing transform (TRT) [34], [35]. These could remove complex RM and DFM by correlation function of echo signal, and achieve coherent integration with low computational load. However, high computational efficiency of these methods is at the cost of detection ability. Moreover, their detection performance is poor at low SNR level.

It is interesting and important to develop high speed maneuvering target detection algorithms with low computational complexity and high detection performance. Compared with the nonlinear transform, the linear transform will not bring about coherent integration performance loss and can be applied in low SNR environment as well [5]. Therefore, as the typical linear transform, the DCFT and its modified forms have been employed for target detection [28], [30]. In addition, the detector based on DCFT is proved to be a likelihood ratio test (LRT) detector which is optimal for rectilinearly moving targets in the presence of Gaussian noise [15], [28]. However, these methods are computationally prohibitive for highly maneuvering motion model since the DCFT involves a multi-dimensional parameter searching procedure. It is well known that fast Fourier transform (FFT) can largely reduce the computational complexity of the discrete Fourier transform (DFT). In essence, the high efficiency of FFT lies in utilizing the inherent symmetry and periodicity of the frequency terms. Based on the concept of decimation-in-time FFT, the fast quadratic phase transform (FQPT) has been proposed to reduce the computational complexity of the QPT [36], [37].

A novel high speed maneuvering target detection algorithm based on fast discrete chirp-Fourier transform (FDCFT) is proposed in this paper. First, the problems faced with ground radar detection are analyzed in detail based on the third-order motion model with jerk. It is shown the linear RM (LRM), undersampled linear DFM (ULDFM) and quadratic DFM (QDFM) must be compensated in order to improve the detection performance. Meanwhile, the velocity ambiguity phenomenon should also be taken into consideration. Second, to solve the migration problems in a fast manner, the KT is first applied to correct RM in range frequency and slow time domain rather than directly perform 4-D search in range time and slow time domain [26], [30]. Noting that the echo signal can be regarded as a cubic phase signal with respect to the slow time at a certain range cell, the FDCFT is proposed to compensate ULDFM and QDFM, and realize the coherent integration for high speed maneuvering target. Since the ADCFT has similar structures with the DFT, we exploit the inherent symmetry and periodicity of searching chirp rate and derivative of chirp rate to present the FDCFT based on the concept of decimation-in-time FFT. Considering that radix-4 decomposition costs fewer complex multiplications than those of radix-2 decomposition [38], we adopt radix-4 decomposition to implement the FDCFT. It is worth noting that the FDCFT does not damage the properties of the ADCFT, and can reduce the computational load. Thereafter, the velocity ambiguity phenomenon is analyzed and well dealt with through constructing corresponding compensation functions. Furthermore, superiority of the proposed method in terms of coherent integration performance, computational complexity and multi-target detection performance, are analyzed in detail. As for higher-order motion model, we analyze the applicability of the proposed method and extend the FDCFT to arbitrary higher-order DFM. Theoretical analysis indicates that the computational savings of the proposed fast method is more significant as the motion model order increases. Compared with the fast detection methods, such

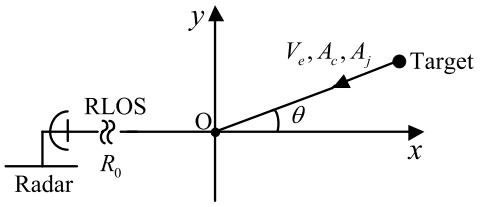


**FIGURE 1.** Motion model of high-speed maneuvering target.

as KT-CPF [31] and TRT-SKT-LVD [34], the proposed algorithm can effectively improve the detection performance at very low SNR. Moreover, the proposed method could achieve a close detection performance but effectively reduce computational cost when compared with GRFT [29].

To easily remember the expressions in this paper, the main abbreviations and symbols are listed as follows:

$\hat{t}$ is the fast time.

$t_m$ is the slow time.

$T$ is the observation time.

$t_a$ is the new slow-time variable after KT.

$f_c$ is the carrier frequency.

$\lambda$ is the wavelength.

$\Gamma_{\text{amb}}$ is the velocity ambiguity degree.

PRF is the pulse repetition frequency.

KT denotes the keystone transform.

RM denotes the range migration.

DFM denotes the Doppler frequency migration.

LRM, SRM, and TRM denote linear, second-order, and third-order range migration, respectively.

LDFM, and QDFM denote the linear and quadratic Doppler frequency migration, respectively.

ULDFM and UQDFM denote the undersampled linear and quadratic Doppler frequency migration, respectively.

DCFT denotes the discrete chirp-Fourier transform.

ADCFT denotes the advanced discrete chirp-Fourier transform.

FDCFT denotes the fast discrete chirp-Fourier transform.

## II. SIGNAL MODEL AND PROBLEM FORMULATION

### A. SIGNAL MODEL

Assume that the linear frequency modulated (LFM) signal is transmitted with narrowband pulse Doppler radar, then the transmitted pulse trains can be expressed as

$$s(\hat{t}, t_m) = \text{rect}(\hat{t}/T_p) \exp\left(j\pi\gamma\hat{t}^2\right) \exp\left[j2\pi f_c\left(\hat{t} + t_m\right)\right] \quad (1)$$

where $\text{rect}(u) = \begin{cases} 1, |u| \le \frac{1}{2} \\ 0, |u| > \frac{1}{2} \end{cases}$, $T_p$ is the pulse width, $f_c$ is the carrier frequency, $\gamma$ is the chirp rate of LFM signal, $\hat{t}$ is the fast time, $t_m \in [-T/2, T/2]$ denotes the slow time, and $T$ is the observation time.

The motion model of high-speed maneuvering target is shown as Fig. 1, where a constant jerk is taken into consideration due to the target's strong maneuverability. The $x$-axis denotes the radar line of sight (RLOS). $\theta$ is the yaw angle. $R_0$, $V_e$, $A_c$ and $A_j$ denote the initial slant range, velocity, acceleration, and jerk, respectively. Thus, the instantaneous slant range of the target with respect to the slow time is expressed as

$$R(t_m) = R_0 - V_e\cos(\theta)t_m - \frac{1}{2}A_c\cos(\theta)t_m^2 - \frac{1}{6}A_j\cos(\theta)t_m^3 \quad (2)$$

Because of the relatively short observation time, $\theta$ can be assumed constant [2]. Then, define $v = V_e\cos(\theta)$, $a_1 = A_c\cos(\theta)$, and $a_2 = A_j\cos(\theta)$, where $v$, $a_1$, and $a_2$ are, respectively, the radial components of the target's initial velocity, acceleration, and jerk. Therefore, the instantaneous slant range in (2) can be rewritten as

$$R(t_m) = R_0 - vt_m - \frac{1}{2}a_1t_m^2 - \frac{1}{6}a_2t_m^3 \quad (3)$$

The received signal of a fast moving target after down conversion can be stated as [32]

$$s_r(\hat{t}, t_m) = \sigma_0\text{rect}\left[\frac{\hat{t} - R(t_m)/c}{T_p}\right]\exp\left[-j4\pi\frac{R(t_m)}{\lambda}\right] \times \exp\left\{j\pi\gamma\left[\hat{t} - \frac{2R(t_m)}{c}\right]^2\right\} \quad (4)$$

where $\sigma_0$ is the target reflectivity and adopted as Swerling V model, $\lambda = c/f_c$ is the wavelength, and $c$ is the light speed.

Performing pulse compression (PC) on the received signal $s_r(\hat{t}, t_m)$, we obtain the compressed signal as

$$s_p(\hat{t}, t_m) = \sigma_1\text{sinc}\left\{B\left[\hat{t} - \frac{2R(t_m)}{c}\right]\right\} \times \exp\left[-j4\pi\frac{R(t_m)}{\lambda}\right] \quad (5)$$

where $\text{sinc}(x) = \sin(\pi x)/(\pi x)$, and $B$ is the bandwidth.

### B. PROBLEM FORMULATION

From (5), we see both the compressed signal envelope and phase terms change with the slow time, which will induce complex RM and DFM for high-speed maneuvering target detection. In the following, the generating mechanisms of RM and DFM are analyzed in detail to formulate the problems for ground-based radar detection.

#### 1) GENERATING MECHANISMS OF RM

Fig. 2 depicts the RM forms according to (5). The RM will occur when the envelope change value $\Delta R(t_m)$ exceeds half a range resolution during the observation time (shown as Fig. 2 (a)), that is,

$$\Delta R(t_m) = |\max[R(t_m)] - \min[R(t_m)]| > \rho_r/2 \quad (6)$$

where $\rho_r = c/(2B)$ is the range resolution, $\max(x)$ and $\min(x)$ denote the maximum and minimum values of $x$, respectively.

Considering the slant range form in (3), the RM may present three forms in theory including linear RM (LRM), second-order RM (SRM) and third-order RM (TRM), which are illustrated in Fig. 2 (a), (b), and (c), respectively. From (6),

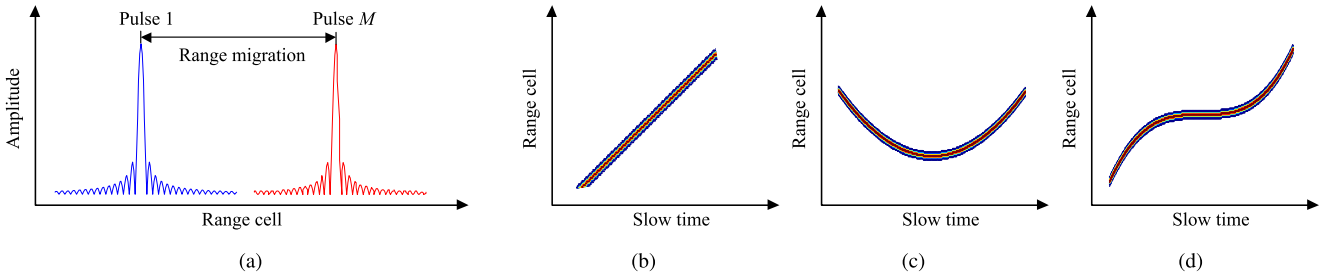


**FIGURE 2.** RM. (a) Definition of RM. (b) LRM. (c) SRM (d) TRM.

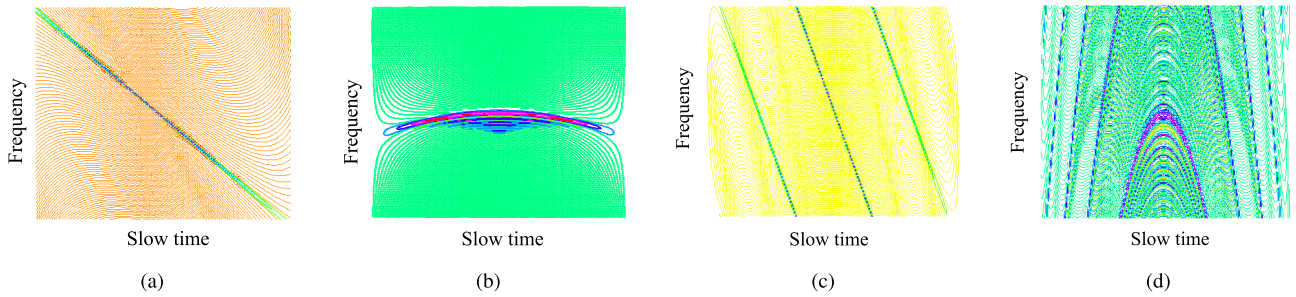


**FIGURE 3.** DFM. (a) LDFM. (b) QDFM. (c) ULDFM (d) UQDFM.

LRM, SRM, and TRM corresponds to the range change value induced by velocity, acceleration, and jerk, respectively, which should satisfy

$$\begin{cases} \Delta R_{\mathrm{LRM}} = |vT| > \rho_r/2 \\ \Delta R_{\mathrm{SRM}} = \left|a_1 T^2/8\right| > \rho_r/2 \\ \Delta R_{\mathrm{TRM}} = \left|a_2 T^3/24\right| > \rho_r/2 \end{cases} \tag{7}$$

where $\Delta R_{\mathrm{LRM}}$, $\Delta R_{\mathrm{SRM}}$, and $\Delta R_{\mathrm{TRM}}$ denote the envelope change value of LRM, SRM and TRM, respectively.

### 2) GENERATING MECHANISMS OF DFM

The Doppler frequency $f_D$ can be expressed as

$$f_D = \frac{2}{\lambda}\frac{dR(t_m)}{dt_m} \tag{8}$$

When the change in Doppler frequency is over half of the Doppler resolution during the observation, the DFM will occur, that is,

$$\Delta f_D = |\max(f_D) - \min(f_D)| > \rho_d/2 \tag{9}$$

where $\rho_d = 1/T$ is the Doppler resolution.

Theoretically, there may exist two forms of DFM with respect to (5), namely linear DFM (LDFM), and QDFM [39], which are respectively depicted in Fig. 3 (a) and (b). LDFM and QDFM are resulted from the variation of acceleration and jerk, respectively, which should satisfy

$$\begin{cases} \Delta f_{\mathrm{LDFM}} = \left|\frac{4a_1 T}{\lambda}\right| > \rho_d \\ \Delta f_{\mathrm{SDFM}} = \left|\frac{a_2 T^2}{2\lambda}\right| > \rho_d \end{cases} \tag{10}$$

where $\Delta f_{\mathrm{LDFM}}$ and $\Delta f_{\mathrm{SDFM}}$ denote the change value of LDFM and QDFM, respectively.

It should be noted that undersampled LDFM (ULDFM) and QDFM (UQDFM) will occur when the sampling frequency in slow domain is less than twofold Doppler frequency change, which are shown in Fig. 3 (c) and (d). Noting that the sampling frequency in slow domain is equal to pulse repetition frequency (PRF), the occurred conditions of ULDFM and UQDFM could be stated as

$$\begin{cases} \Delta f_{\mathrm{LDFM}} > \mathrm{PRF}/2 \\ \Delta f_{\mathrm{SDFM}} > \mathrm{PRF}/2 \end{cases} \tag{11}$$

In order to realize the long-range detection with ground-based radar, three typical characteristics should be noted: 1) the observation time should be prolonged to improve integration gain, which extends as long as second level [22]. 2) high range resolution is not required, and hundreds of meters are enough [31]. 3) the PRF is usually low to guarantee no range ambiguity, which is usually selected as a few hundred Hz [2], [23]. Based on the above characteristics, the practical RM and DFM with ground-based radar are analyzed in detail, which are shown in Fig. 4. Since the velocity of high-speed target is usually as high as kilometers per second, especially for hypersonic aircrafts in near space, the LRM must be considered according to constrained velocity as shown in Fig. 4 (a). Considering the strong maneuverability is around ten times the force of gravity, the SRM and TRM are slight, and could be ignored as analyzed in Fig. 4 (b) and (c). Similarly, the LDFM and QDFM should be taken into consideration because the needed acceleration and jerk shown in Fig. 4 (d) and (e) are within

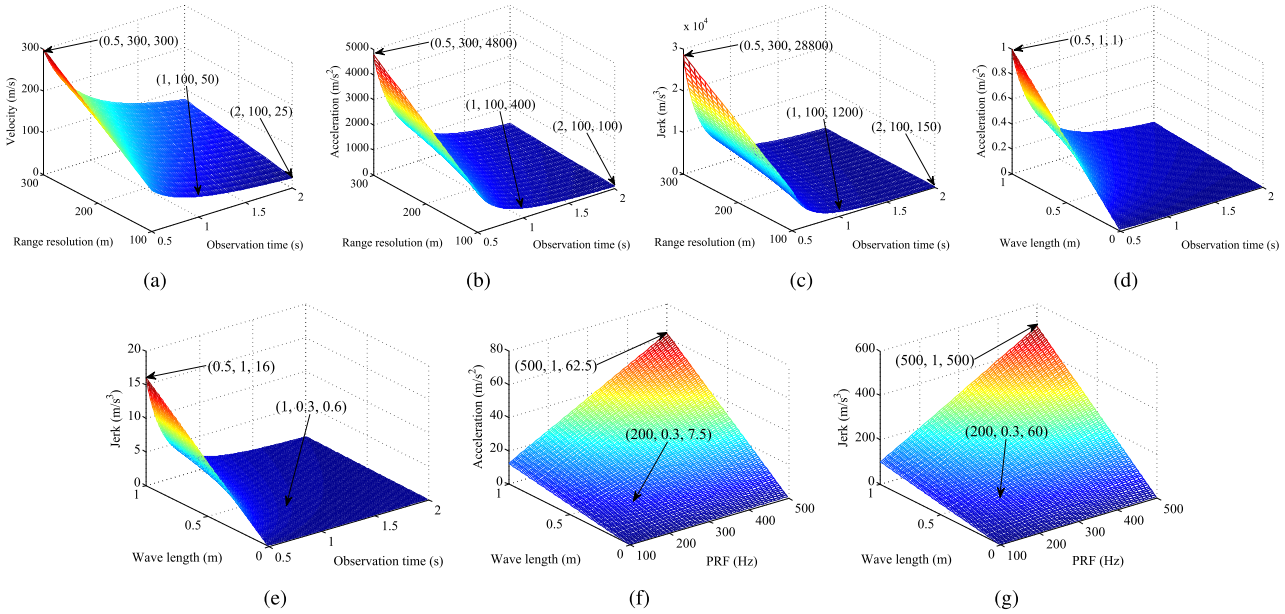


**FIGURE 4.** RM and DFM analysis with the ground-based detection radar. (a) Parameters constraint for LRM. (b) Parameters constraint for SRM. (c) Parameters constraint for TRM. (d) Parameters constraint for LDFM. (e) Parameters constraint for QDFM. (f) Parameters constraint of ULDFM when T=1 s. (g) Parameters constraint for UQDFM when T=1 s.

the scope of strong maneuverability. Moreover, Fig. 4 (f) and (g) give the constraint parameters of ULDFM and UQDFM, respectively, from which we conclude that the ULDFM should be considered, and UQDFM could be ignored in most cases.

## III. RADAR HIGH-SPEED MANEUVERING TARGET DETECTION ALGORITHM

### A. LRM COMPENSATION VIA KT

First, perform FFT on (5) along fast time axis, and change the compressed signal into range frequency-slow time domain,

$$s_p(f, t_m) = \sigma_2 \mathrm{rect}\left(\frac{f}{B}\right) \exp\left[-j\frac{4\pi\,(f+f_c)}{c}\,(R_0 - vt_m)\right] \times \exp\left[j\frac{4\pi(f+f_c)}{c}\left(\frac{1}{2}a_1 t_m^2 + \frac{1}{6}a_2 t_m^3\right)\right] \quad (12)$$

In (12), the essence of RM effect lies in the couple term between slow time and range frequency. Since KT could effectively decouple the first-order term regardless of the target's velocity in the low SNR condition [5], [12], we first apply KT to remove the LRM effect. The KT is a resampling process and expressed as

$$t_m = \frac{f_c}{f+f_c} t_a \quad (13)$$

where $t_a$ denotes the new slow-time variable.

Substituting (13) into (12) yields

$$s_k(f, t_a) = \sigma_2 \mathrm{rect}\left(\frac{f}{B}\right) \exp\left[-j\frac{4\pi}{c}\,(f+f_c)\,R_0\right] \times \exp\left(j\frac{4\pi}{\lambda}vt_a\right) \exp\left[j\frac{2\pi a_1 t_a^2}{\lambda\,(1+f/f_c)}\right] \times \exp\left[j\frac{2\pi a_2 t_a^3}{3\lambda\,(1+f/f_c)^2}\right] \quad (14)$$

With respect to a narrowband signal, $f \ll f_c$ is satisfied. Then performing the Taylor series expansion on (14), and we can obtain

$$s_k(f, t_a) \approx \sigma_2 \mathrm{rect}\left(\frac{f}{B}\right) \exp\left[-j\frac{4\pi}{c}\,(f+f_c)\,R_0\right] \times \exp\left(j\frac{4\pi}{\lambda}vt_a\right) \exp\left[j\frac{2\pi a_1 t_a^2}{\lambda}\left(1-\frac{f}{f_c}\right)\right] \times \exp\left[j\frac{2\pi a_2 t_a^3}{3\lambda}\left(1-\frac{2f}{f_c}\right)\right] \quad (15)$$

After performing the range inverse Fourier transform (IFT) on (15), one has

$$s_k(\hat{t}, t_a) = \sigma_3 \mathrm{sinc}\left[B\left(\hat{t} - \frac{2R_0}{c} - \frac{a_1 t_a^2}{c} - \frac{2a_2 t_a^3}{3c}\right)\right] \times \exp\left[-j\frac{4\pi}{\lambda}\left(R_0 - vt_a - \frac{1}{2}a_1 t_a^2 - \frac{1}{6}a_2 t_a^3\right)\right] \quad (16)$$

It is noted from (16) that the LRM is effectively compensated by KT whereas the SRM and TRM still exist. Meanwhile, the second-order and third-order slow time forms in the exponential term of (16) may result in the LDFM and QDFM. Based on the analysis in Section II-B, the residual SRM and TRM could be ignored while the ULDFM and QDFM must be considered for the long-range detection with ground-based

radar. Then (16) could be rewritten as

$$s_k(\hat{t}, t_a) \approx \sigma_3 \mathrm{sinc}\left[B\left(\hat{t}-\frac{2R_0}{c}\right)\right] \times \exp\left[-j\frac{4\pi}{\lambda}\left(R_0 - vt_a - \frac{1}{2}a_1 t_a^2 - \frac{1}{6}a_2 t_a^3\right)\right] \quad (17)$$

With the fast time sampling interval $T_s$ and slow time sampling interval $T_a$, the discrete form of (17) is stated as

$$s_k(n, m) = \sigma_3 \mathrm{sinc}\left[B\left(nT_s - \frac{2R_0}{c}\right)\right] \times \exp\left(-j\frac{4\pi}{\lambda}R_0\right) s(m) \quad (18)$$

where

$$s(m) = \exp\left\{j2\pi\left[f_d m T_a + \frac{1}{2}b_1 (mT_a)^2 + \frac{1}{6}b_2 (mT_a)^3\right]\right\} \quad (19)$$

$f_d$, $b_1$, and $b_2$ respectively denote center frequency, chirp rate, and derivative of chirp rate, which are determined by

$$\begin{cases} f_d = 2v/\lambda \\ b_1 = 2a_1/\lambda \\ b_2 = 2a_2/\lambda \end{cases} \quad (20)$$

### B. ULDFM AND QDFM COMPENSATION BASED ON FDCFT

#### 1) INTRODUCTION OF ADCFT

In fact, the ULDFM and QDFM effect can be regarded as a cubic phase signal with respect to the slow time. In [10], [32], and [40], the CPF, MICPF, and GHHAF are proposed to compensate the complex DFM effect. The main principle of these methods is to utilize the time delay to obtain a reduced-order signal model, and further realize the DFM compensation based on fast parameter estimation of the cubic signal. However, these methods involve nonlinear transforms, which have a high requirement for input SNR, and lead to great performance loss. In order to improve the ultimate detection performance in low SNR circumstance, we have proposed a compensation method based on ADCFT [30], which can be expressed as

$$S_{\mathrm{ADCFT}}(k, l, p) = \frac{1}{\sqrt{M}}\sum_{m=0}^{M-1} s(m) W_m^{km+\frac{lM}{2f_a^2}m^2+\frac{pM}{6f_a^3}m^3} \quad (21)$$

where $f_a = 1/T_a$ is sample frequency of $s(m)$, $k$, $l$, and $p$ denote respectively the searching digital center frequency, chirp rate, derivative of chirp rate, and $W_M^k = e^{-j2\pi k/M}$.

By means of ADCFT, the ULDFM and QDFM can be simultaneously compensated when the searching parameters match with the corresponding parameters of the cubic phase signal. Because of the linear transform, ADCFT does not have the input SNR threshold and bring about performance loss. Meanwhile, compared with the DCFT [41], it overcomes the limit of the prime sampling number and suppresses the 'picket fence' effect.

However, it should be noted that the ADCFT is computationally prohibitive due to 3-D search procedure. The required complex multiplications (CM) of the direct searching computation of the ADCFT are

$$N_{\mathrm{direct}} = M^2 N_l N_p \quad (22)$$

where $N_l$ and $N_p$ denote the numbers of searching chirp rate and derivative of chirp rate, respectively.

Considering the symmetry and periodicity of the searching center frequency term in (21), the ADCFT is implemented as

$$S_{\mathrm{ADCFT}}(k, l, p) = \frac{1}{\sqrt{M}}\mathrm{FFT}_m\left[s(m) W_m^{\frac{lM}{2f_a^2}m^2+\frac{pM}{6f_a^3}m^3}\right] \quad (23)$$

where $\mathrm{FFT}_m$ denotes FFT along $m$.

Using the FFT, the CM of ADCFT are reduced to

$$N_{\mathrm{FFT}} = \frac{1}{2}MN_lN_p \log_2^M \quad (24)$$

However, the symmetry and periodicity of the searching chirp rate and derivative of chirp rate are not exploited in (21) and (23). It has been proved that the redundancy along chirp rate axis could be utilized to decimate the signal according to the decimation-in-time FFT concept [36], [37], [42]. Meanwhile, the radix-2 and radix-4 decomposition are most commonly used algorithms with respect to FFT computation, and radix-4 decomposition costs fewer complex multiplications than those of radix-2 decomposition [38]. Motivated by the radix-4 based FFT, we propose the FDCFT based on radix-4 decomposition to further reduce the computational load of ADCFT in the following section.

#### 2) THE PRINCIPLE OF FDCFT

Assume $M = 4^q$, where $q$ is an integer. For presentation, define a demodulated sequence

$$x_q^{(l,p)}(m) = s(m) W_m^{\frac{lM}{2f_a^2}m^2+\frac{pM}{6f_a^3}m^3} = s(m) e^{-j2\pi\left[(l/N_l)m^2+(p/N_p)m^3\right]} \quad (25)$$

where $N_l = 2f_a^2$, $N_p = 6f_a^3$, $l = 0, 1, ..., N_l$, and $p = 0, 1, ..., N_p$. For easy analysis, the intervals of searching chirp rate and derivative of chirp rate are set to 1 here. Meanwhile, it should be noted that $N_p \geqslant N_l \geqslant M$ can be generally satisfied. Then, the ADCFT of $s(m)$ can be expressed as

$$S_{\mathrm{ADCFT}}(k, l, p) = \frac{1}{\sqrt{M}}\mathrm{DFT}_m\left[x_q^{(l,p)}(m)\right] \quad (26)$$

Since $M = 4^q$, the computation of ADCFT can be decomposed into $q$ stages based on radix-4 decomposition. Without considering the constant coefficient $1/\sqrt{M}$, the computation of demodulated sequence at the $r$th stage is described as

$$g_r^{(l,p)}(k) = \mathrm{DFT}_u\left[x_q^{(l,p)}(4^r u + s)\right] = \sum_{u=0}^{M/4^r-1} x_q^{(l,p)}(4^r u + s) W_{M/4^r}^{uk} \quad (27)$$

where $u = 0, 1, ..., M/4^r$, $s = 0, 1, ..., 4^r - 1$, $r = 0, 1, ..., q-1$.

Using the symmetry and periodicity of searching chirp rate and derivative of chirp rate in the ADCFT, we obtain (28) (at the bottom of this page), where $a_l, a_p = 0, 1, 2, 3$, $\psi(s) = 2a_l s + 3a_p s^2$, $v$ is a nonnegative integer, and

$$g_{r+1,i}^{(l,p)}(k) = \sum_{u=0}^{M/4^{r+1}-1} x_q^{(l,p)}[4^{r+1}u + (i-1)4^r + s]W_{M/4^{r+1}}^{uk}, \quad i = 1, 2, 3, 4. \tag{29}$$

It is observed from (28) that a long demodulated sequence with $M/4^r$ points at the $r$th stage can be decomposed into four short sequences with $M/4^{(r+1)}$ points at the $r+1$th stage. Meanwhile, the computation of $g_r^{(l,p)}(k)$ for $l = l_0 + a_l N_l/4^{(r+1)}$ and $p = p_0 + a_p N_p/4^{(r+1)}$ can be implemented by $g_r^{(l,p)}(k)$ for $l = l_0$ and $p = p_0$. Therefore, based on radix-4 decomposition, FDCFT is realized via firstly computing $g_r^{(l,p)}(k)$ for small values of $l$ and $p$ at a high stage and thereafter computing $g_r^{(l,p)}(k)$ for larger values of $l$ and $p$ at a lower stage according to (28).

When $a_l = a_p = 0$, (28) can be simplified as

$$g_r^{(l,p)}(k) = g_{r+1,1}^{(l,p)}(k) + W_{M/4^r}^{k} g_{r+1,2}^{(l,p)}(k) + W_{M/4^r}^{2k} g_{r+1,3}^{(l,p)}(k) + W_{M/4^r}^{3k} g_{r+1,4}^{(l,p)}(k) \tag{30}$$

By further utilizing the symmetry and periodicity of $k$, we obtain (31) (at the bottom of this page), where $k = 0, 1, ..., M/4^{r+1} - 1$. It should be noted that (31) is a basic computing unit of radix-4 decomposition and further computation can be performed on demodulated sequences until 4-points DFTs are obtained. Moreover, with respect to other values of $a_l$ and $a_p$ (i.e. $a_l, a_p = 0, 1, 2, 3$), the modified basic computing unit can be easily obtained by multiplying (31) with phase factors $e^{-j2\pi(a_l s^2 + a_p s^3)/4^{r+1}}$.

### 3) COMPUTATIONAL COMPLEXITY OF FDCFT

The main computational steps of the FDCFT are first given and then the corresponding complex multiplications are analyzed in each step, which can be described as follows:

Step 1) Compute the demodulated sequence $x_q^{(l,p)}(m)$ for $l = 0, 1, ..., N_l/M - 1$ and $p = 0, 1, ..., N_p/M - 1$. It should be noted that no CM are needed when $l = 0$ and $p = 0$. Therefore, the required CM involved in Step 1 are

$$\begin{aligned} N_{\text{step1}} &= M(N_l/M - 1)(N_p/M - 1) \\ &= N_l N_p/M - N_l - N_p + M \end{aligned} \tag{32}$$

Step 2) For $a_l = a_p = 0$, compute the $g_r^{(l,p)}(k)$ at each stage according to (31). Since the multiplier factor of basic computing unit only contains $\pm 1$ and $\pm j$, no CM are needed at $q-1$th stage. Thus, the required CM involved in Step 2 are

$$\begin{aligned} N_{\text{step2}} &= \frac{3}{4} M \sum_{r=0}^{q-2} \frac{N_l N_p}{(4^{r+1})^2} \\ &= \frac{1}{20}\left[1 - \left(\frac{1}{16}\right)^{q-2}\right] M N_l N_p \end{aligned} \tag{33}$$

Step 3) Compute the complex multiplications needed for the phase factors $e^{-j2\pi(a_l s^2 + a_p s^3)/4^{r+1}}$ in (28) with other values of $a_l$ and $a_p$. Because of no multiplications are required when $r = 0$, the computational load in this step is

$$\begin{aligned} N_{\text{step3}} &= \frac{3}{4} M \sum_{r=1}^{q-1} \frac{15 N_l N_p}{(4^{r+1})^2} \\ &= \frac{3}{64}\left[1 - \left(\frac{1}{16}\right)^{q-1}\right] M N_l N_p \end{aligned} \tag{34}$$

Based on the above analysis, the total CM needed in the FDCFT are

$$\begin{aligned} N_{\text{FDCFT}} &= N_{\text{step1}} + N_{\text{step2}} + N_{\text{step3}} \\ &= N_l N_p/M - N_l - N_p + M \end{aligned}$$

$$g_r^{(l+a_l N_l/4^{r+1}, p+a_p N_p/4^{r+1})}(k) = \begin{cases} e^{-j2\pi(a_l s^2 + a_p s^3)/4^{r+1}}\left[g_{r+1,1}^{(l,p)}(k) + W_{M/4^r}^{k} g_{r+1,2}^{(l,p)}(k) + W_{M/4^r}^{2k} g_{r+1,3}^{(l,p)}(k) + W_{M/4^r}^{3k} g_{r+1,4}^{(l,p)}(k)\right], & \text{if } \psi(s) = 4v; \\ e^{-j2\pi(a_l s^2 + a_p s^3)/4^{r+1}}\left[g_{r+1,1}^{(l,p)}(k) - jW_{M/4^r}^{k} g_{r+1,2}^{(l,p)}(k) - W_{M/4^r}^{2k} g_{r+1,3}^{(l,p)}(k) + jW_{M/4^r}^{3k} g_{r+1,4}^{(l,p)}(k)\right], & \text{if } \psi(s) = 4v+1; \\ e^{-j2\pi(a_l s^2 + a_p s^3)/4^{r+1}}\left[g_{r+1,1}^{(l,p)}(k) - W_{M/4^r}^{k} g_{r+1,2}^{(l,p)}(k) + W_{M/4^r}^{2k} g_{r+1,3}^{(l,p)}(k) - W_{M/4^r}^{3k} g_{r+1,4}^{(l,p)}(k)\right], & \text{if } \psi(s) = 4v+2; \\ e^{-j2\pi(a_l s^2 + a_p s^3)/4^{r+1}}\left[g_{r+1,1}^{(l,p)}(k) + jW_{M/4^r}^{k} g_{r+1,2}^{(l,p)}(k) - W_{M/4^r}^{2k} g_{r+1,3}^{(l,p)}(k) - jW_{M/4^r}^{3k} g_{r+1,4}^{(l,p)}(k)\right], & \text{if } \psi(s) = 4v+3. \end{cases} \tag{28}$$

$$\begin{bmatrix} g_r^{(l,p)}(k) \\ g_r^{(l,p)}(k + M/4^{r+1}) \\ g_r^{(l,p)}(k + 2M/4^{r+1}) \\ g_r^{(l,p)}(k + 3M/4^{r+1}) \end{bmatrix} = \begin{bmatrix} 1 & 1 & 1 & 1 \\ 1 & -j & -1 & j \\ 1 & -1 & 1 & -1 \\ 1 & j & -1 & -j \end{bmatrix} \begin{bmatrix} g_{r+1,1}^{(l,p)}(k) \\ g_{r+1,2}^{(l,p)}(k) W_{M/4^r}^{k} \\ g_{r+1,3}^{(l,p)}(k) W_{M/4^r}^{2k} \\ g_{r+1,4}^{(l,p)}(k) W_{M/4^r}^{3k} \end{bmatrix} \tag{31}$$

$$+\left[\frac{31}{320}-\frac{271}{5120}\left(\frac{1}{16}\right)^{q-2}\right]MN_lN_p \approx \frac{31}{320}MN_lN_p \tag{35}$$

The ratio of the computational complexity of the ADCFT using FFT to that of FDCFT is

$$\frac{N_{\text{FFT}}}{N_{\text{FDCFT}}} = \frac{MN_lN_p\log_2^M/2}{31MN_lN_p/320} \approx 5.2\log_2^M \tag{36}$$

The ratio of the computational complexity of the direct computation of the ADCFT to that of FDCFT is

$$\frac{N_{\text{direct}}}{N_{\text{FDCFT}}} = \frac{M^2N_lN_p}{31MN_lN_p/320} \approx 10.3M \tag{37}$$

From (36) and (37), we know that the FDCFT could reduce the computational load largely compared to the ADCFT by direct computation and using FFT.

#### 4) COHERENT INTEGRATION VIA FDCFT

Performing FDCFT on (18), the high speed maneuvering target energy will be well integrated in ADCFT domain when the searching parameters are accurately matched, i.e.,

$$G_n(f_dM/f_a, b_1, b_2) = \sigma_3\sqrt{M}\,\text{sinc}\left[B\left(nT_s-\frac{2R_0}{c}\right)\right] \times \exp\left(-j\frac{4\pi}{\lambda}R_0\right) \tag{38}$$

where $G_n(k,l,p)$ denotes the coherent integration result.

Therefore, the estimated number of range cell $\hat{n}$, digital center frequency $\hat{k}$, chirp rate $\hat{l}$, and derivative of chirp rate $\hat{p}$ can be obtained by the following expression

$$(\hat{n},\hat{k},\hat{l},\hat{p}) = \arg\max_{n,k,l,p}|G_n(k,l,p)| \tag{39}$$

Then the motion parameters $R_0$, $v$, $a_1$, and $a_2$ are estimated as

$$\begin{cases}\hat{R_0}=\hat{n}c/(2B)\\ \hat{v}=\hat{k}f_a\lambda/(2M)\\ \hat{a_1}=\hat{l}\lambda/2\\ \hat{a_2}=\hat{p}\lambda/2\end{cases} \tag{40}$$

### C. PROCESSING STRATEGY OF VELOCITY AMBIGUITY PHENOMENON

Because of the high speed and low PRF, velocity ambiguity phenomenon may occur [2], [17]. Then, the target velocity is rewritten as

$$v = \Gamma_{\text{amb}}v_a + v_0 \tag{41}$$

where $v_a = \lambda\text{PRF}/2$ is the blind velocity, $\Gamma_{\text{amb}}$ is the velocity ambiguity degree, and $v_0$ is the unambiguous velocity which satisfies $|v_0| < v_a/2$.

Since the KT is a resampling and interpolation process, the velocity ambiguity will result in the occurrence of half blind velocity effect [43] and invalid correction of the LRM [5], which would bring about great performance loss, and thus should be well dealt with.

#### 1) ELIMINATION OF HALF BLIND VELOCITY EFFECT

The sinc-interpolation processing is used to realize the implementation of KT in this paper because of its robustness and little performance loss [7]. However, the sinc-interplotion will suffer a great performance loss near the odd times of half blind velocity when velocity ambiguity occurs, which is called half blind velocity effect [43], [44]. As for the proposed algorithm, the half blind velocity effect will make detection performance degraded when the velocity satisfies

$$\frac{c(\Gamma_{\text{amb}}+0.5)\text{PRF}}{2(f_c+B/2)} < v < \frac{c(\Gamma_{\text{amb}}+0.5)\text{PRF}}{2(f_c-B/2)} \tag{42}$$

In this case, the velocity ambiguity degree at the frequency component $-B/2$ is different from that at the frequency component $B/2$, which may also bring about estimation error of the velocity. To eliminate the half blind velocity effect, the inter-pulse compensation function is constructed as

$$h_1(t_m) = \exp\left[-j2\pi\,(-\text{PRF}/2)\,t_m\right] \tag{43}$$

The new form of radar echoes can be obtained by multiplying (4) with (43), i.e.,

$$s_r'(\hat{t},t_m) = s_r(\hat{t},t_m)h_1(t_m) \tag{44}$$

#### 2) COMPENSATION OF LRM INDUCED BY VELOCITY AMBIGUITY

Substituting (41) into (12) yields

$$s_p(f,t_m) = \sigma_2\text{rect}\left(\frac{f}{B}\right)h_2(f,t_m) \times \exp\left[-j\frac{4\pi\,(f+f_c)}{c}(R_0-vt_m)\right] \times \exp\left[j\frac{4\pi(f+f_c)}{c}\left(\frac{1}{2}a_1t_m^2+\frac{1}{6}a_2t_m^3\right)\right] \tag{45}$$

where

$$h_2(f,t_m) = \exp\left[j\frac{4\pi\,(f+f_c)}{c}v_at_m\Gamma_{\text{amb}}\right] = \exp\left(j\frac{4\pi f}{c}v_at_m\Gamma_{\text{amb}}\right)\exp\left(j2\pi\,\text{PRF}\Gamma_{\text{amb}}t_m\right) = \exp\left(j\frac{4\pi f}{c}v_at_m\Gamma_{\text{amb}}\right) \tag{46}$$

Performing KT on (45) and then expanding the transform result according to Taylor series expansion, one can obtain

$$s_k(f,t_a) = \sigma_2\text{rect}\left(\frac{f}{B}\right)\exp\left[-j\frac{4\pi}{c}(f+f_c)R_0\right] \times \exp\left(j\frac{4\pi}{\lambda}v_0t_a\right)\exp\left[j\frac{2\pi a_1t_a^2}{\lambda}\left(1-\frac{f}{f_c}\right)\right] \times \exp\left[j\frac{2\pi a_2t_a^3}{3\lambda}\left(1-\frac{2f}{f_c}\right)\right]h_2(f,t_a) \tag{47}$$

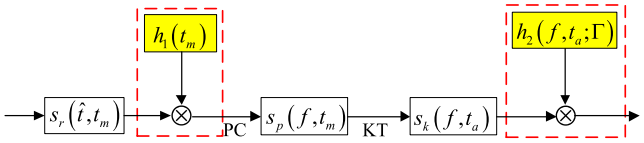


**FIGURE 5.** The main processing flow of solving the velocity ambiguity phenomenon.

where

$$\begin{aligned} h_2(f,t_a) &= \exp\left(j\frac{4\pi}{\lambda}\frac{1}{1+f/f_c}v_a t_a \Gamma_{\text{amb}}\right) \\ &\approx \exp\left(-j2\pi f \text{PRF}\Gamma_{\text{amb}} t_a/f_c\right) \\ &\quad \times \exp\left(j2\pi f \text{PRF}\Gamma_{\text{amb}} t_a\right) \\ &\approx \exp\left(-j2\pi f \text{PRF}\Gamma_{\text{amb}} t_a/f_c\right) \end{aligned} \tag{48}$$

It is observed from (48) that the LRM induced by the velocity ambiguity phenomenon could not be effectively removed through KT. To solve this problem, a velocity ambiguity degree compensation function is constructed as

$$h_2(f,t_a;\Gamma) = \exp\left(j2\pi f \text{PRF}\Gamma t_a/f_c\right) \tag{49}$$

where $\Gamma$ is the searching velocity ambiguity.

Multiplying (47) with (49), one has

$$\begin{aligned} s_k(f,t_a) &= \sigma_2 \text{rect}\left(\frac{f}{B}\right)\exp\left[-j\frac{4\pi}{c}(f+f_c)R_0\right] \\ &\quad \times \exp\left(j\frac{4\pi}{\lambda}v_0 t_a\right)\exp\left[j\frac{2\pi a_1 t_a^2}{\lambda}\left(1-\frac{f}{f_c}\right)\right] \\ &\quad \times \exp\left[j\frac{2\pi a_2 t_a^3}{3\lambda}\left(1-\frac{2f}{f_c}\right)\right] \\ &\quad \times \exp\left[-j2\pi f \text{PRF}(\Gamma_{\text{amb}}-\Gamma)t_a/f_c\right] \end{aligned} \tag{50}$$

From (50), we see that the LRM induced by the velocity ambiguity phenomenon will be removed when $\Gamma = \Gamma_{\text{amb}}$. Then, (39) and (40) can be rewritten as

$$(\hat{n},\hat{\Gamma},\hat{k},\hat{l},\hat{p}) = \arg\max_{n,\Gamma,k,l,p}\left|G_{n,\Gamma}(k,l,p)\right| \tag{51}$$

$$\begin{cases} \hat{R}_0 = \hat{n}c/(2B) \\ \hat{v} = \hat{k}f_a\lambda/(2M) + \hat{\Gamma}v_a \\ \hat{a_1} = \hat{l}\lambda/2 \\ \hat{a_2} = \hat{p}\lambda/2 \end{cases} \tag{52}$$

where $G_{n,\Gamma}(k,l,p)$ denotes the coherent integration result when velocity ambiguity phenomenon occurs.

In summary, the main steps to solve the velocity ambiguity phenomenon include constructing the inter-pulse compensation function $h_1(t_m)$ and the velocity ambiguity degree compensation function $h_2(f,t_a;\Gamma)$, which are shown in Fig. 5. It should be noted that the coherent integration result $G_{n,\Gamma}(k,l,p)$ differ from true center frequency by PRF/2, and thus the result should be corrected by shifting PRF/2 along center frequency direction.

### D. PROCEDURE OF PROPOSED DETECTION ALGORITHM

The procedure of proposed detection algorithm can be summarized as follows:

Step 1: Perform demodulation and pulse compression on the received raw echoes, and the signal $s_p(f,t_m)$ in range frequency and slow time domain is obtained.

Step 2: Apply the KT in (13) to $s_p(f,t_m)$, and the signal is transformed to $s_k(f,t_a)$.

Step 3: Determine the searching scope of the velocity ambiguity degree $[\Gamma_1,\Gamma_2]$, chirp rate $[l_1,l_2]$, and derivative of chirp rate $[p_1,p_2]$ based on relative prior information such as moving status of the targets to be detected. The interval $\Delta l$ and interval $\Delta p$ can be determined by Doppler resolution [27], that is, $\Delta l = 1/T^2$ and $\Delta p = 4/T^3$.

Step 4: Construct the velocity ambiguity degree compensation function to remove the residual RM and perform IFFT in range-frequency domain.

Step 5: Carry out the FDCFT in all range bins to achieve the coherent integration.

Step 6: Repeat Steps 4 and 5 until all the velocity ambiguity degrees in Step 3 are searched, and obtain the maximum peak value of coherent integration result $G_{n_0,\Gamma_0}(k_0,l_0,p_0)$. Set $l = l_0$, $p = p_0$, and $\Gamma = \Gamma_0$, and construct the detection map $G_{n,\Gamma_0}(k,l_0,p_0)$ in the range-Doppler domain.

Step 7: Take $|G_{n_0,\Gamma_0}(k_0,l_0,p_0)|$ as the test statistic and employ the biparametric constant false alarm ratio (CFAR) detector to obtain the adaptive threshold $\eta$ based on the detection map [22]. Compare the test statistic with the adaptive threshold to confirm a target, which can be expressed as

$$\left|G_{n_0,\Gamma_0}(k_0,l_0,p_0)\right| \underset{H_0}{\overset{H_1}{\gtrless}} \eta \tag{53}$$

Therefore, the flowchart of the proposed detection algorithm is shown in Fig. 6.

In order to eliminate the half blind velocity effect, the operating steps marked with dashed box in Fig. 6 should make some changes. First, the radar echoes after demodulation should be changed according to (44) in Step 1. Second, when constructing the detection map in Step 6, the result based on the new form of radar echoes should be shifted PRF/2 along center frequency direction, which is denoted as $\left|G'_{n,\Gamma_0}(k,l_0,p_0)\right|$. Finally, choose the larger value between $\left|G_{n,\Gamma_0}(k,l_0,p_0)\right|$ and $\left|G'_{n,\Gamma_0}(k,l_0,p_0)\right|$ as the element of the detection map.

## IV. PERFORMANCE ANALYSIS OF PROPOSED ALGORITHM

In this part, the performance of the proposed algorithm is analyzed in detail, which would reflect the superiority of the proposed method in the aspects of coherent integration gain, computational complexity, and multi-target detection.

### A. COHERENT INTEGRATION GAIN ANALYSIS

Here, the output SNR is adopted to illustrate the coherent integration gain since it is generally utilized as the performance

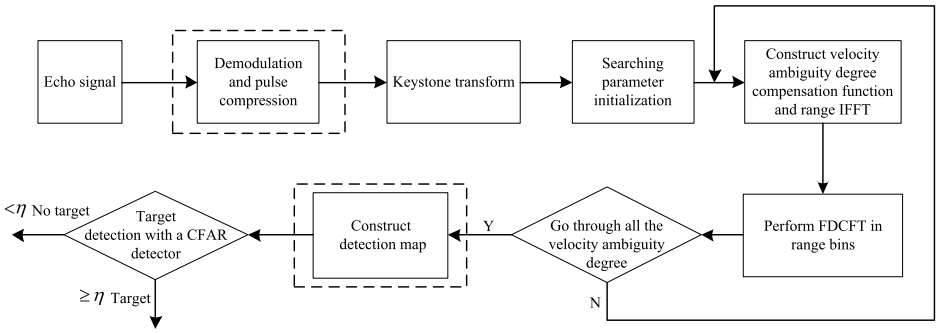


**FIGURE 6.** Flowchart of proposed detection algorithm.

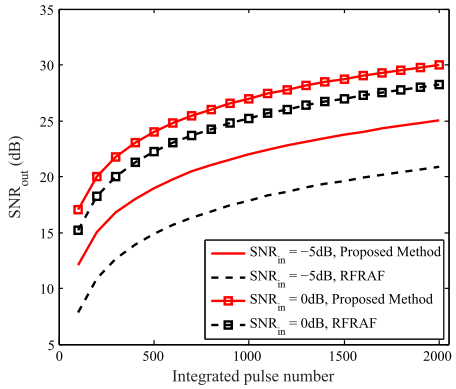


**FIGURE 7.** Relation between integrated pulse number and $\mathrm{SNR_{out}}$ of proposed method and RFRAF. (PRF = 500 Hz, $B = 1$ MHz, $v = 3000$ m/s, $a_1 = 30$ m/s$^2$, and $a_2 = 20$ m/s$^3$ ).

indicator in radar system [22]. Suppose the performance loss induced by the interpolation of the KT is not considered at first. The output SNR of the proposed method at the peak location $(k_0, l_0, p_0)\,|_{n_0,\Gamma_0}$ is defined as follows [22], [27]

$$\mathrm{SNR}_{\mathrm{out}}^{\mathrm{proposed}} = \frac{|Z_s\,(k_0, l_0, p_0)|^2}{\mathrm{var}\,[Z_x\,(k_0, l_0, p_0)]} \tag{54}$$

where $Z_s\,(k_0, l_0, p_0) = |G_s\,(k_0, l_0, p_0)|^2$ is the output power of target, $Z_x\,(k_0, l_0, p_0) = |G_{s+n}\,(k_0, l_0, p_0)|^2$ denotes the output power of target plus noise, and var[·] represents the variance calculation.

According to Appendix, one can obtain

$$\mathrm{SNR}_{\mathrm{out}}^{\mathrm{proposed}} = \frac{M^3\mathrm{SNR}_{\mathrm{in}}^2}{2M^2\mathrm{SNR}_{\mathrm{in}} - M + 2} \tag{55}$$

where $\mathrm{SNR_{in}}$ is the input SNR of the proposed method.

Compared with the output SNR of RFRAF $\mathrm{SNR}_{\mathrm{out}}^{\mathrm{RFRAF}}$, which is defined in [27], then we obtain

$$\mathrm{SNR}_{\mathrm{out}}^{\mathrm{proposed}} > \mathrm{SNR}_{\mathrm{out}}^{\mathrm{RFRAF}} \tag{56}$$

The relation between integrated pulse number and $\mathrm{SNR_{out}}$ of the proposed method and RFRAF, respectively, is shown in Fig. 7 for different $\mathrm{SNR_{in}}$ ($\mathrm{SNR_{in}} = -5$ dB and 0 dB). Clearly, the $\mathrm{SNR_{out}}$ of both methods increase with the integrated pulse number, and larger $\mathrm{SNR_{in}}$ acquires a better $\mathrm{SNR_{out}}$. Moreover, the proposed method obtains a higher $\mathrm{SNR_{out}}$ than that of the RFRAF under the same conditions of integrated pulse number and input SNR. In addition, as the input SNR decreases, the $\mathrm{SNR_{out}}$ gap between the proposed method and RFRAF increase. Thus, the coherent integration performance of the proposed method is superior than that of RFRAF. Compared with the GRFT, the proposed method suffers a slight integration performance loss, which is caused by the interpolation of the KT [7]. It is worth noting that the integration gain analysis of the proposed method is on the basis of no RM caused by acceleration and jerk occurring. Fortunately, this condition can usually be satisfied for long-range surveillance radar [17], [31].

### B. COMPUTATIONAL COMPLEXITY ANALYSIS

The computational complexity of the proposed method, GRFT, RFRAF, and KT-CPF is analyzed in terms of CM. Denote the numbers of echo pulses, searching range cells, searching velocity, searching acceleration, searching jerk, searching velocity ambiguity degree, and searching rotation angle by $M, N_r, N_v, N_{a_1}, N_{a_2}, N_\Gamma$, and $N_p$, respectively. Since the interpolation operation is applied to realize the KT, $N_r M^2$ CM are needed. $N_\Gamma(MN_r \log_2^{N_r}/2+31MN_rN_{a_1}N_{a_2}/320)$ CM are needed for FFT along fast time and the FDCFT. On the other hand, $N_rMN_vN_{a_1}N_{a_2}$ CM are needed for the GRFT algorithm [5], [40]. According to [45], we get $N_v = MN_\Gamma$. Thereafter, the computational cost of the proposed method is $O(N_\Gamma N_r N_{a_1} N_{a_2} M)$ whereas the computational burden of GRFT is $O(N_\Gamma N_r N_{a_1} N_{a_2} M^2)$, which suggests that the computational complexity of the proposed method is largely reduced compared with the GRFT. Meanwhile, the RFRAF needs $O[N_rN_\Gamma N_{a_1}N_{a_2}M(M + N_p(8M + 6M\log_2^{2M}))]$ CM. Only $O[N_rM^2 + N_\Gamma MN_r(\log_2^{N_r}/2 + 2) + 6N_{a_1}N_r(M + 1)]$ CM are needed with respect to KT-CPF [40]. The detailed computational complexities of the above algorithms are listed in Table 1. It is worth noting that the KT-CPF algorithm is more computationally efficient than that of the above algorithms since the motion parameters of the target could be estimated step by step. However, the KT-CPF algorithm will suffer performance loss and the error propagation effect because of its nonlinearity, and cannot work in low SNR environment.

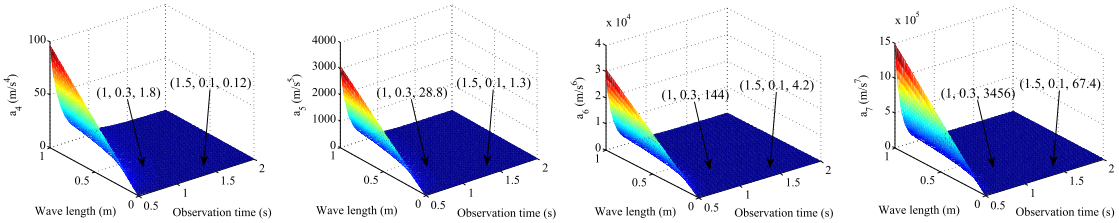


**FIGURE 8.** High-order DFM analysis. (a) Parameters constraint for fourth-order DFM. (b) Parameters constraint for fifth-order DFM. (c) Parameters constraint for sixth-order DFM. (d) Parameters constraint for seventh-order DFM.

**TABLE 1.** Comparison of computational complexity.

| Method | Multiplications |
|---|---|
| Proposed | $O[N_r M^2 + N_\Gamma M N_r(\log_2^{N_r}/2 + 31 N_{a_1} N_{a_2}/320)]$ |
| GRFT | $O(N_\Gamma N_r N_{a_1} N_{a_2} M^2)$ |
| RFRAF | $O[N_r N_\Gamma N_{a_1} N_{a_2} M(M + N_p(8M + 6M\log_2^{2M}))]$ |
| KT-CPF | $O[N_r M^2 + N_\Gamma M N_r(\log_2^{N_r}/2 + 2) + 6N_{a_1} N_r(M+1)]$ |

### C. MULTI-TARGET DETECTION PERFORMANCE ANALYSIS

In above analysis, the presented method shows superiority in detecting a high speed maneuvering target. However, there may exist multiple targets in a real scenario, which could be divided into three kinds: multiple targets with different motion parameters, multiple targets with some same motion parameters, and multiple targets with significantly different intensities [28]. The presented method could have a multi-target detection performance since the KT and FDCFT are both linear transforms. When multiple targets have different motion parameters, they are located in different range cells, and could be detected and distinguished by searching range cells. As for multiple targets with some same motion parameters, they can be detected and distinguished by residual different motion parameters. For example, there are two targets with same range cell and acceleration in the scenario. They can be distinguished in different searching velocity ambiguity degrees, center frequencies or derivative of chirp rates. In addition, the side-lobes of strong targets may submerge the weak ones when multiple targets have remarkably different intensities, which will make the detection performance degraded. In this condition, the CLEAN technique [46] could be first applied to eliminate the influences of strong targets, and then the coherent integration of different targets can be achieved iteratively. It is worth noting that the blind-speed side lobe (BSSL) may be produced in the GRFT method and may lead to false alarm and loss detections in a real multi-target scenario [7]. Moreover, the RFRAF and KT-CPF methods may suffer from cross-term interference due to their nonlinearities, and thus the detection performance will be influenced to some extent.

## V. APPLICATION TO HIGHER-ORDER MOTION MODEL

Many literatures indicate that the higher-order motion model is more accurate to describe the strong maneuverability of target [29], [35]. For the motion model with $J$-th order, the instantaneous slant range is expressed as

$$R(t_m) = R_0 - \sum_{j=1}^{J} \frac{1}{j!} a_j t_m^j \tag{57}$$

where $a_j$ denotes the target motion parameter with $j$-th order.

Based on (6) and (9), the critical values of $j$-th order motion parameter causing RM and DFM, i.e., $a_{jR}$ and $a_{jF}$, are respectively denoted as

$$a_{jR} = \begin{cases} \dfrac{j! 2^{j-2} \rho_r}{T^j}, & j \text{ is odd;} \\ \dfrac{j! 2^{j-1} \rho_r}{T^j}, & j \text{ is even.} \end{cases} \tag{58}$$

$$a_{jF} = \begin{cases} \dfrac{\lambda (j-1)! 2^{j-3}}{T^j}, & j \text{ is odd;} \\ \dfrac{\lambda (j-1)! 2^{j-4}}{T^j}, & j \text{ is even.} \end{cases} \tag{59}$$

Comparing (58) with (59), we find that DFM is more easy to generate than that of RM for $j$-th order motion parameter. Meanwhile, we also obtain

$$\begin{cases} \dfrac{a_{j+2R}}{a_{jR}} = \dfrac{4(j+2)(j+1)}{T^2} \\ \dfrac{a_{j+2F}}{a_{jF}} = \dfrac{4j(j+1)}{T^2} \end{cases} \tag{60}$$

It is seen from (60) that $\{a_{jR}\}$ and $\{a_{jF}\}$ are incremental when $j > T/2$. For high-order motion model, $j > T/2$ is generally satisfied. Thus, the occurrence of $j$-th order RM and DFM become more difficult as the order $j$ increases. Based on the analysis of Section II-B, we conclude that the $j$-th order RM can be ignored but the $j$-th order DFM may occur for $j > 3$. Fig. 8 illustrates the high-order DFM analysis with $j = 4, 5, 6, 7$, where the fourth- and fifth-order DFM will easily occur for short wavelength and long observation time. The proposed detection algorithm is based on the third-order motion model, which can achieve general precision requirement. However, for higher-order motion model, the proposed method will suffer from detection performance loss due to higher-order DFMs. In order to improve the applicability to the higher-motion model, we can extend the FDCFT to arbitrary higher order. Define a $J$-th order demodulated sequence as

$$x_q^{(l_2,\ldots,l_J)}(m) = s(m) e^{-j2\pi \sum_{j=2}^{J} (l_j/N_j) m^j} \tag{61}$$

where $l_j = 0, 1, 2, \ldots, N_j - 1$.

**TABLE 2. Computational procedures and complexities of extended FDCFT.**

| Step | Description | Computational cost |
|---|---|---|
| 1) | Compute the demodulated sequence $x_q^{(l_2,\ldots,l_J)}(m)$ for $l_j = 0, 1, \ldots, N_j/M - 1$ according to (61). | $N_{\text{step1}} = M\Pi_{j=2}^{J}(N_j/M - 1)$ |
| 2) | For $a_j = 0$, compute the $g_r^{(l_2,\ldots,l_J)}(k)$ at each stage according to (65). | $N_{\text{step2}} = \frac{3}{4}M\sum_{r=0}^{q-2}\Pi_{j=2}^{J}\frac{N_j}{4^{r+1}}$ |
| 3) | Compute the complex multiplications needed for the phase factors in (63) with other values of $a_j$. | $N_{\text{step3}} = \frac{45}{4}M\sum_{r=1}^{q-1}\Pi_{j=2}^{J}\frac{N_j}{4^{r+1}}$ |

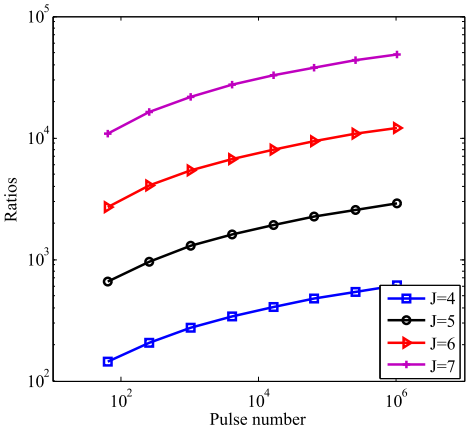


**FIGURE 9. Comparison of computational complexity.**

According to (27), the computation of demodulated sequence at the $r$-th stage is modified as

$$g_r^{(l_2,\ldots,l_J)}(k) = \sum_{u=0}^{M/4^r-1} x_q^{(l_2,\ldots,l_J)}[4^r u + s]W_{M/4^r}^{uk} \quad (62)$$

Exploiting the symmetry and periodicity of motion parameters of different orders, we can obtain (63) (at the bottom of this page), where $\phi_J(s) = e^{-j2\pi\sum_{j=2}^{J}a_j s^j/4^{r+1}}$, $a_j = 0, 1, 2, 3$, $\psi_J(s) = \sum_{j=2}^{J} j a_j s^{j-1}$, and

$$g_{r+1,i}^{(l_2,\ldots,l_J)}(k) = \sum_{u=0}^{M/4^{r+1}-1} x_q^{(l_2,\ldots,l_J)}[4^{r+1}u + (i-1)4^r + s]W_{M/4^{r+1}}^{uk}, \quad i = 1, 2, 3, 4. \quad (64)$$

From (63), we can see the computation of $g_r^{(l_2,\ldots,l_J)}(k)$ for $l_j = l_{0j} + a_j N_j/4^{r+1} (j = 2, 3, \ldots, J)$ can be implemented by $g_r^{(l_2,\ldots,l_J)}(k)$ for $l_j = l_{0j}$. Based on radix-4 decomposition, extended FDCFT for $J$-th order motion model can be obtained by first computing $g_r^{(l_2,\ldots,l_J)}(k)$ for small values of $l_j$ at a high stage and then computing $g_r^{(l_2,\ldots,l_J)}(k)$ for larger values of $l_j$ at a lower stage according to (63). Assuming $a_j = 0$ and exploiting the symmetry and periodicity of $k$, we can further get (65) (at the bottom of next page), where $k = 0, 1, \ldots, M/4^{r+1} - 1$.

The computational procedures and complexities of the extended FDCFT are shown in Table 2.

Fig. 9 illustrates the ratio between the computational complexities needed by using FFT and the proposed fast method for compensating the fourth to seventh-order DFM. Since more redundancy along different dimensions of motion parameters is exploited, the savings achieved through the proposed fast method are more significant as the order of DFM or pulse number $M$ increases.

**TABLE 3. Simulation parameters of radar system.**

| Parameter | Value |
|---|---|
| Carrier frequency | 3 GHz |
| Pulse repetition frequency | 200 Hz |
| Bandwidth | 1 MHz |
| Sample frequency | 1 MHz |
| Pulse duration | 100 us |
| Coherent integration time | 1.28 s |

## VI. NUMERICAL RESULTS

In this section, numerical simulations are presented to verify the effectiveness of the proposed algorithm for high-speed maneuvering target detection with jerk motion, where the parameters of the radar system are listed in Table 3.

$$g_r^{(l_2+a_2N_l/4^{r+1},\ldots,l_J+a_JN_J/4^{r+1})}(k) = \begin{cases} \phi_J(s)\left[g_{r+1,1}^{(l_2,\ldots,l_J)}(k) + W_{M/4^r}^{k} g_{r+1,2}^{(l_2,\ldots,l_J)}(k) + W_{M/4^r}^{2k} g_{r+1,3}^{(l_2,\ldots,l_J)}(k) + W_{M/4^r}^{3k} g_{r+1,4}^{(l_2,\ldots,l_J)}(k)\right], \text{if } \psi_J(s) = 4v; \\ \phi_J(s)\left[g_{r+1,1}^{(l_2,\ldots,l_J)}(k) - jW_{M/4^r}^{k} g_{r+1,2}^{(l_2,\ldots,l_J)}(k) - W_{M/4^r}^{2k} g_{r+1,3}^{(l_2,\ldots,l_J)}(k) + jW_{M/4^r}^{3k} g_{r+1,4}^{(l_2,\ldots,l_J)}(k)\right], \text{if } \psi_J(s) = 4v+1; \\ \phi_J(s)\left[g_{r+1,1}^{(l_2,\ldots,l_J)}(k) - W_{M/4^r}^{k} g_{r+1,2}^{(l_2,\ldots,l_J)}(k) + W_{M/4^r}^{2k} g_{r+1,3}^{(l_2,\ldots,l_J)}(k) - W_{M/4^r}^{3k} g_{r+1,4}^{(l_2,\ldots,l_J)}(k)\right], \text{if } \psi_J(s) = 4v+2; \\ \phi_J(s)\left[g_{r+1,1}^{(l_2,\ldots,l_J)}(k) + jW_{M/4^r}^{k} g_{r+1,2}^{(l_2,\ldots,l_J)}(k) - W_{M/4^r}^{2k} g_{r+1,3}^{(l_2,\ldots,l_J)}(k) - jW_{M/4^r}^{3k} g_{r+1,4}^{(l_2,\ldots,l_J)}(k)\right], \text{if } \psi_J(s) = 4v+3. \end{cases} \quad (63)$$

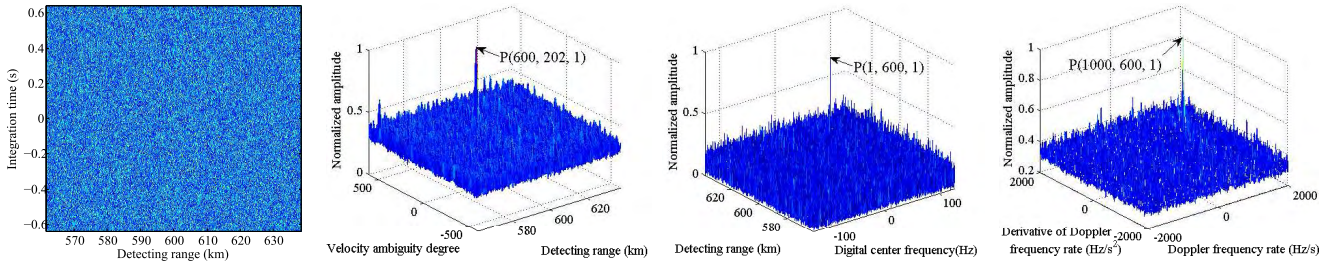


**FIGURE 10.** Detection result for a high-speed maneuvering target. (a) Result after PC. (b) Projection of detection result in fold factor-range domain. (c) Projection of detection result in range-Doppler frequency domain. (d) Projection of detection result in Doppler frequency rate-derivative Doppler frequency rate domain.

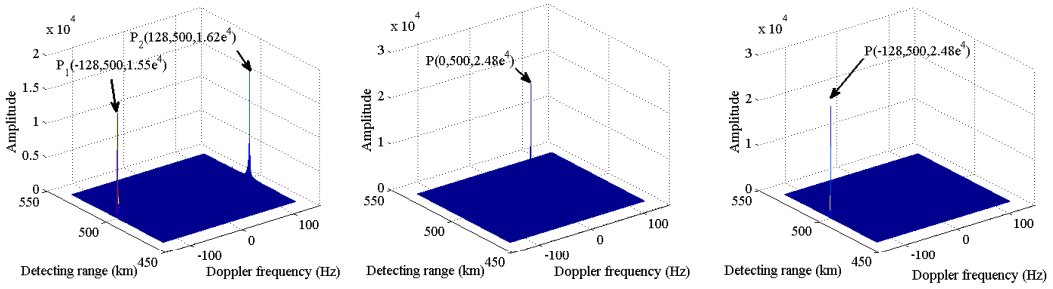


**FIGURE 11.** Detection result for a high-speed maneuvering target with half blind velocity effect. (a) Detection result for the target with $v = 2025$ m/s by the proposed method directly. (b) Detection result for the target with $v = 2020$ m/s by the proposed method. (c) Detection result for the target with $v = 2025$ m/s after eliminating half blind velocity effect.

### A. DETECTION ABILITY OF PROPOSED METHOD

The first simulation is carried out to verify the single target detection ability, where the motion parameters of the target are set as $R_0 = 600$ km, $v = 2020$ m/s, $a_1 = 50$ m/s$^2$, $a_2 = 30$ m/s$^3$, and the intput SNR is $-25$ dB. The results are shown in Fig. 10.

It can be seen from Fig. 10 (a) that the signal after PC is submerged in the noise. By processing with the proposed method, peaks are clearly formed in Figs. 10 (b), (c), and (d), which represent respective projections of detection result in different ADCFT domains. As seen in Section III, the target energy can be well accumulated when the searching motion parameters are respectively matched with real ones. From Figs. 10 (b), (c), and (d), the matched motion parameters are obtained as $\hat{R}_0 = 600$ km, $\hat{\Gamma}_{\text{amb}} = 202$, $\hat{k} = 1$, $\hat{l} = 1000$, and $\hat{p} = 600$. According to (52), the corresponding motion parameters can be calculated as $\hat{v} = 2020.8$ m/s, $\hat{a}_1 = 50$ m/s$^2$, and $\hat{a}_2 = 30$ m/s$^3$. We can obtain that the estimated results align with the true values.

In the following simulation, a target with half blind velocity effect is considered without noise for clarity of presentation. The target motion parameters are set as $R_0 = 500$ km, $v = 2025$ m/s, $a_1 = 30$ m/s$^2$, and $a_2 = 15$ m/s$^3$. It should be noted that (42) is satisfied with simulated parameters and half blind velocity effect would occur. In order to better illustrate the half blind velocity effect, another target without half blind velocity ($v = 2020$ m/s) is also simulated for comparison.

Fig. 11 (a) shows the coherent integration results of a target with half blind velocity effect. It is seen that the energy of the target is dispersed into two Doppler frequency cells and two peaks are formed in range-Doppler domain. When the CFAR detection technology is utilized in successive processing, the number of the targets could not be accurately determined, and the detection performance will degrade. A detection result of a target without half blind velocity effect is shown in Fig. 11 (b). Compared with the peak values in Fig. 11 (a) and (b), the peak value loss of target with the half blind velocity effect is about 2 dB, which has an

$$\begin{bmatrix} g_r^{(l_2,\ldots,l_J)}(k) \\ g_r^{(l_2,\ldots,l_J)}(k+M/4^{r+1}) \\ g_r^{(l_2,\ldots,l_J)}(k+2M/4^{r+1}) \\ g_r^{(l_2,\ldots,l_J)}(k+3M/4^{r+1}) \end{bmatrix} = \begin{bmatrix} 1 & 1 & 1 & 1 \\ 1 & -j & -1 & j \\ 1 & -1 & 1 & -1 \\ 1 & j & -1 & -j \end{bmatrix} \begin{bmatrix} g_{r+1,1}^{(l_2,\ldots,l_J)}(k) \\ g_{r+1,2}^{(l_2,\ldots,l_J)}(k) W_{M/4^r}^{k} \\ g_{r+1,3}^{(l_2,\ldots,l_J)}(k) W_{M/4^r}^{2k} \\ g_{r+1,4}^{(l_2,\ldots,l_J)}(k) W_{M/4^r}^{3k} \end{bmatrix} \tag{65}$$

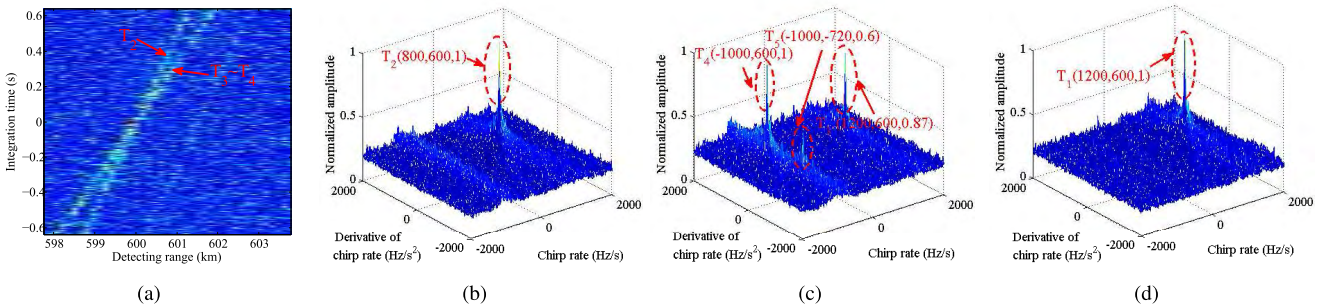


**FIGURE 12.** Detection results for multiple high-speed maneuvering targets. (a) Result after PC. (b) Detection result for $T_2$ with searching slant range $R_0 = 600$ km and velocity ambiguity degree $\Gamma = 200$. (c) Detection result for $T_3$, $T_4$, $T_5$ with searching slant range $R_0 = 600$ km and velocity ambiguity degree $\Gamma = 300$. (d) Detection result for $T_1$ with searching slant range $R_0 = 601.5$ km and velocity ambiguity degree $\Gamma = 200$.

obvious effect on detection performance. Fig. 11 (c) shows the detection result after eliminating half blind velocity effect. Clearly, the energy of the target can be well accumulated and the peak value is close to that without the half blind velocity effect.

The subsequent test is performed to evaluate the multiple target detection ability. The motion parameters of targets are listed in Table 4. The simulation results are shown in Fig. 12.

The result after PC is shown in Fig. 12 (a), where only two bright lines are formed. The motion trajectories of targets $T_1$ and $T_5$ cannot emerge due to their low SNRs. Meanwhile, because of the same initial slant range and radial velocity, the motion trajectories of targets $T_3$ and $T_4$ are overlapped. The detection result for $T_2$ is shown in Fig. 12 (b). Although $T_2$, $T_3$, $T_4$, and $T_5$ are located at the same range cell (i.e., 600 km) at the start, $T_2$ could be detected and distinguished by searching velocity ambiguity degree $\Gamma = 200$. Because of the same initial slant range and radial velocity, $T_3$, $T_4$, and $T_5$ cannot be differentiated via searching range cell and velocity ambiguity degree. Fortunately, they are different in radial acceleration and jerk, which are distinguishable by different chirp rates and derivative of chirp rates. The detection result of $T_3$, $T_4$, and $T_5$ is shown in Fig. 12 (c), where three peaks are formed in the chirp rate-derivative of chirp rate domain. Thereafter, $T_3$, $T_4$, and $T_5$ can be detected using peak detection and CFAR technique, and the corresponding motion parameters of the targets could be obtained according to (52). Fig. 12 (d) shows the detection result for $T_1$ with searching slant range $R_0 = 601.5$ km and velocity ambiguity degree $\Gamma = 200$. An obvious peak is generated in the chirp rate-derivative of chirp rate domain. Thus, the proposed method has a good ability of detecting multiple targets.

### B. COMPARISON WITH OTHER EXISTING METHODS

In this simulation, the computational complexity of the proposed method is evaluated in comparison with that of the GRFT, RFRAF, and KT-CPF. In order to cover the range of common high speed maneuvering target motion parameters, the searching scope of initial slant range, radial velocity, radial acceleration, and radial jerk are set as [200, 600] km, $[-6000, 6000]$ m/s, $[-200, 200]$ m/s$^2$, and $[-200, 200]$ m/s$^3$,

**TABLE 4.** Motion parameters of multiple targets.

| Motion parameter | $T_1$ | $T_2$ | $T_3$ | $T_4$ | $T_5$ |
|---|---|---|---|---|---|
| Initial slant range (km) | 601.5 | 600 | 600 | 600 | 600 |
| Radial velocity (m/s) | 2000 | 2000 | 3000 | 3000 | 3000 |
| Radial acceleration (m/s$^2$) | 60 | 40 | 60 | -50 | -50 |
| Radial jerk (m/s$^2$) | 30 | 30 | 30 | 30 | -36 |
| SNR (dB) | -20 | -15 | -18 | -16 | -22 |

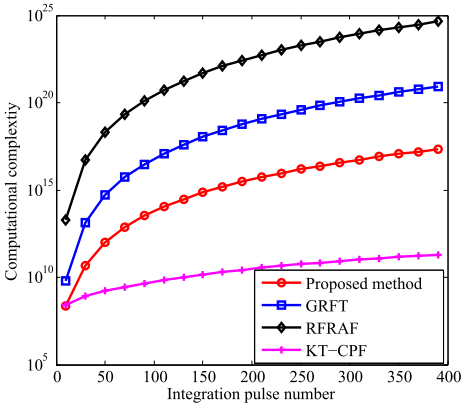


**FIGURE 13.** Computational complexity of proposed method, GRFT, RFRAF and KT-CPF versus pulse number.

respectively. Fig. 13 shows the computational complexity of the proposed method, GRFT, RFRAF, and KT-CPF versus pulse number. It can be seen the proposed method has a relatively lower computational burden than that of the RFRAF and GRFT methods, and the computational complexity of the proposed method changes more slowly with integrated pulse number. Although the KT-CPF has the lowest computational complexity, it cannot work well in low SNR environment because of nonlinearity.

The last simulation is performed to demonstrate the detection performance of the proposed method in different SNR levels, where the RFT, RFRFT, RFRAF, KT-CPF, and GRFT are used for comparison. The initial slant range, radial velocity, acceleration, and jerk of the target are 600 km, 3600 m/s, 100 m/s$^2$, and 90 m/s$^3$, respectively. Additionally, the CFAR detector is combined with the above six methods as

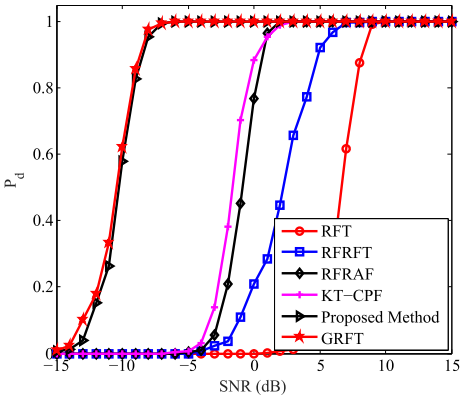


**FIGURE 14.** Detection probability of RFT, RFRFT, RFRAF, KT-CPF, proposed method and GRFT when $P_{fa} = 10^{-4}$.

corresponding detectors, and the constant false alarm probability $P_{fa}$ is set as $10^{-4}$. The added SNRs after pulse compression are SNR = [−15:1:15] dB, and in each case, 500 times of Monte Carlo simulations are done. Fig. 14 shows the detection probability of the six methods versus different SNR level. It can be seen the presented method can obtain close detection performance as that of the GRFT and the performance loss is less than 1 dB. The KT-CPF and RFRAF have a lower antinoise performance in comparison with the presented method and the performance loss is approximately 8 dB because of their nonlinearities and propagation errors. Moreover, although the RFRFT and RFT are the optimal detectors for constant acceleration and uniform motion model, respectively, they suffer from great performance loss since the QDFM is not considered. Combined with the analysis of Fig. 13, we conclude that the proposed method can make a good balance between detection performance and computational cost.

## VII. CONCLUSION

This paper has presented a novel method for high speed maneuvering target based on FDCFT, which could compensate the RM, ULDFM and QDFM simultaneously, and realize the coherent integration for the targets with ground-based radar. The characteristics of the proposed method are summarized as follows: 1) It makes full use of the motion characteristic and can achieve a coherent integration without the RM and DFM effects. 2) It can eliminate the half blind velocity effect and correct the LRM induced by the interpolation of KT and the velocity ambiguity phenomenon. 3) It could be applied to multi-target scenario because of its linear property. 4) It has a better detection performance than some typical coherent integration methods such as RFT, RFRFT, RFRAF, and KT-CPF in low SNR case. 5) It can acquire high estimation performance in low SNR case with a relatively lower computational cost in comparison with the GRFT. 6) It can be extended to an arbitrary higher-order motion model with great computational advantage. Theoretical analysis and simulated results have demonstrated the effectiveness of the presented method.

## APPENDIX

Suppose $n(t)$ is the zero-mean, stationary, white complex Gaussian noise with auto-correlation function

$$R_n(\tau) = E\left[n(t)n^*(t+\tau)\right] = \sigma_n^2\delta(\tau) \tag{66}$$

According to (21), the peak value of $Z_s(k_0, l_0, p_0)$ can be expressed as

$$Z_s(k_0, l_0, p_0) = |G_s(k_0, l_0, p_0)|^2 = M\sigma_3^2 \tag{67}$$

Then, the input SNR is defined as $\mathrm{SNR}_{\mathrm{in}} = \sigma_3^2/\sigma_n^2$.

The expected value of $Z_x(k_0, l_0, p_0)$ can be calculated as follows

$$\begin{aligned} &E\left[Z_x(k_0, l_0, p_0)\right] \\ &= E\left[\left|G_s(k_0, l_0, p_0) + G_n(k_0, l_0, p_0)\right|^2\right] \\ &= E\left[\left|G_s(k_0, l_0, p_0)\right|^2\right] + E\left[\left|G_n(k_0, l_0, p_0)\right|^2\right] \\ &\quad + 2\mathrm{Re}\left[G_s(k_0, l_0, p_0)G_n^*(k_0, l_0, p_0)\right] \\ &= \left|G_s(k_0, l_0, p_0)\right|^2 + E\left[\left|G_n(k_0, l_0, p_0)\right|^2\right] \\ &= M\sigma_3^2 + \sigma_n^2 \end{aligned} \tag{68}$$

The variance in (54) is

$$\begin{aligned} &\mathrm{var}\left[Z_x(k_0, l_0, p_0)\right] \\ &= E\left\{\left[Z_x(k_0, l_0, p_0) - E\left[Z_x(k_0, l_0, p_0)\right]\right]^2\right\} \\ &= E\left[\left|G_s(k_0, l_0, p_0)\right|^4\right] - \left\{E\left[\left|G_s(k_0, l_0, p_0)\right|^2\right]\right\}^2 \\ &\quad + 2\left|G_s(k_0, l_0, p_0)\right|^2 E\left[\left|G_s(k_0, l_0, p_0)\right|^2\right] \\ &= 2M\sigma_3^2\sigma_n^2 + \frac{2}{M}\sigma_n^4 - \sigma_n^4 \end{aligned} \tag{69}$$

Then rewriting (54) with the use of (67) and (69), and the output SNR of proposed method can be obtained, that is, (55).

## REFERENCES

[1] C. Jian-Jun, C. Juan, and W. Sheng-Li, "Detection of ultra-high speed moving target based on matched Fourier transform," in *Proc. CIE Int. Conf. Radar*, Shanghai, China, Oct. 2006, pp. 1–4.

[2] M. Xing, J. Su, G. Wang, and Z. Bao, "New parameter estimation and detection algorithm for high speed small target," *IEEE Trans. Aerosp. Electron. Syst.*, vol. 47, no. 1, pp. 214–224, Jan. 2011.

[3] S. Zhu, G. Liao, D. Yang, and H. Tao, "A new method for radar high-speed maneuvering weak target detection and imaging," *IEEE Geosci. Remote Sens. Lett.*, vol. 11, no. 7, pp. 1175–1179, Jul. 2014.

[4] J. Xu, J. Yu, Y.-N. Peng, and X.-G. Xia, "Radon-Fourier transform for radar target detection, I: Generalized Doppler filter bank," *IEEE Trans. Aerosp. Electron. Syst.*, vol. 47, no. 2, pp. 1186–1202, Apr. 2011.

[5] P. Huang, G. Liao, Z. Yang, X.-G. Xia, J.-T. Ma, and J. Ma, "Long-time coherent integration for weak maneuvering target detection and high-order motion parameter estimation based on keystone transform," *IEEE Trans. Signal Process.*, vol. 64, no. 15, pp. 4013–4026, Aug. 2016.

[6] J. Zheng, T. Su, W. Zhu, X. He, and Q. H. Liu, "Radar high-speed target detection based on the scaled inverse Fourier transform," *IEEE J. Sel. Topics Appl. Earth Observ. Remote Sens.*, vol. 8, no. 3, pp. 1108–1119, Mar. 2015.

[7] L. Kong, X. Li, G. Cui, W. Yi, and Y. Yang, "Coherent integration algorithm for a maneuvering target with high-order range migration," *IEEE Trans. Signal Process.*, vol. 63, no. 17, pp. 4474–4486, Sep. 2015.

[8] L. Wu, X. Wei, D. Yang, H. Wang, and X. Li, "ISAR imaging of targets with complex motion based on discrete chirp Fourier transform for cubic chirps," *IEEE Trans. Geosci. Remote Sens.*, vol. 50, no. 10, pp. 4201–4212, Oct. 2012.

[9] J. Zheng, T. Su, L. Zhang, W. Zhu, and Q. H. Liu, "ISAR imaging of targets with complex motion based on the chirp rate–quadratic chirp rate distribution," *IEEE Trans. Geosci. Remote Sens.*, vol. 52, no. 11, pp. 7276–7289, Nov. 2014.
[10] P. Huang, G. Liao, Z. Yang, X.-G. Xia, J. Ma, and J. Zheng, "Ground maneuvering target imaging and high-order motion parameter estimation based on second-order keystone and generalized Hough-HAF transform," *IEEE Trans. Geosci. Remote Sens.*, vol. 55, no. 1, pp. 320–335, Jan. 2017.
[11] S. Yuan, T. Wu, M. Mao, G. Mei, and X. Wei, "Application research of keystone transform in weak high-speed target detection in low-PRF narrowband Chirp radar," in *Proc. 9th Int. Conf. Signal Process.*, Beijing, China, Oct. 2008, pp. 2452–2456.
[12] S. S. Zhang, T. Zeng, T. Long, and H.-P. Yuan, "Dim target detection based on keystone transform," in *Proc. IEEE Int. Radar Conf.*, Arlington, VA, USA, May 2005, pp. 889–894.
[13] P. Huang *et al.*, "A coherent integration method for moving target detection using frequency agile radar," *IEEE Geosci. Remote Sens. Lett.*, to be published. [Online]. Available: https://ieeexplore.ieee.org/document/8478652, doi: 10.1109/LGRS.2018.2870869.
[14] J. Xu, J. Yu, Y.-N. Peng, and X.-G. Xia, "Radon–Fourier transform for radar target detection (II): Blind speed sidelobe suppression," *IEEE Trans. Aerosp. Electron. Syst.*, vol. 47, no. 4, pp. 2473–2489, Oct. 2011.
[15] J. Yu, J. Xu, Y.-N. Peng, and X.-G. Xia, "Radon–Fourier transform for radar target detection (III): Optimality and fast implementations," *IEEE Trans. Aerosp. Electron. Syst.*, vol. 48, no. 2, pp. 991–1004, Apr. 2012.
[16] J. Zheng, T. Su, H. Liu, G. Liao, Z. Liu, and Q. H. Liu, "Radar high-speed target detection based on the frequency-domain deramp-keystone transform," *IEEE J. Sel. Topics Appl. Earth Observ. Remote Sens.*, vol. 9, no. 1, pp. 285–294, Jan. 2016.
[17] J. Su, M. Xing, G. Wang, and Z. Bao, "High-speed multi-target detection with narrowband radar," *IET Radar, Sonar Navigat.*, vol. 4, no. 4, pp. 595–603, Aug. 2010.
[18] R. Tao, N. Zhang, and Y. Wang, "Analysing and compensating the effects of range and Doppler frequency migrations in linear frequency modulation pulse compression radar," *IET Radar, Sonar Navigat.*, vol. 5, no. 1, pp. 12–22, Jan. 2011.
[19] X. Rao, H. Tao, J. Su, J. Xie, and X. Zhang, "Detection of constant radial acceleration weak target via IAR-FRFT," *IEEE Trans. Aerosp. Electron. Syst.*, vol. 51, no. 4, pp. 3242–3253, Oct. 2015.
[20] P. Huang, X.-G. Xia, X. Liu, and G. Liao, "Refocusing and motion parameter estimation for ground moving targets based on improved axis rotation-time reversal transform," *IEEE Trans. Comput. Imag.*, vol. 4, no. 3, pp. 479–494, Sep. 2018.
[21] J. Tian, W. Cui, Q. Shen, Z. Wei, and S. Wu, "High-speed maneuvering target detection approach based on joint RFT and keystone transform," *Sci. China Inf. Sci.*, vol. 56, no. 6, pp. 1–13, Jun. 2013.
[22] X. Chen, J. Guan, N. Liu, and Y. He, "Maneuvering target detection via Radon-fractional Fourier transform-based long-time coherent integration," *IEEE Trans. Signal Process.*, vol. 62, no. 4, pp. 939–953, Feb. 2014.
[23] X. Li, G. Cui, W. Yi, and L. Kong, "Coherent integration for maneuvering target detection based on Radon–Lv's distribution," *IEEE Signal Process. Lett.*, vol. 22, no. 9, pp. 1467–1471, Sep. 2015.
[24] Z. Sun, X. Li, W. Yi, G. Cui, and L. Kong, "Detection of weak maneuvering target based on keystone transform and matched filtering process," *Signal Process.*, vol. 140, pp. 127–138, Nov. 2017.
[25] X. Li, G. Cui, L. Kong, and W. Yi, "Fast non-searching method for maneuvering target detection and motion parameters estimation," *IEEE Trans. Signal Process.*, vol. 64, no. 9, pp. 2232–2244, May 2016.
[26] X. Chen, J. Guan, Y. Huang, N. Liu, and Y. He, "Radon-linear canonical ambiguity function-based detection and estimation method for marine target with micromotion," *IEEE Trans. Geosci. Remote Sens.*, vol. 53, no. 4, pp. 2225–2240, Apr. 2015.
[27] X. Chen, Y. Huang, N. Liu, J. Guan, and Y. He, "Radon-fractional ambiguity function-based detection method of low-observable maneuvering target," *IEEE Trans. Aerosp. Electron. Syst.*, vol. 51, no. 2, pp. 815–833, Apr. 2015.
[28] X. Rao, H. Tao, J. Xie, J. Su, and W. Li, "Long-time coherent integration detection of weak manoeuvring target via integration algorithm, improved axis rotation discrete chirp-Fourier transform," *IET Radar, Sonar Navigat.*, vol. 9, no. 7, pp. 917–926, Jul. 2015.
[29] J. Xu, X.-G. Xia, S.-B. Peng, J. Yu, Y.-N. Peng, and L.-C. Qian, "Radar Maneuvering Target Motion Estimation Based on Generalized Radon-Fourier Transform," *IEEE Trans. Signal Process.*, vol. 60, no. 12, pp. 6190–6201, Dec. 2012.
[30] X. Huang, S. Tang, L. Zhang, S. Li, and C. Lin, "Low-observable maneuvering target detection based on Radon-advanced discrete chirp Fourier transform," in *Proc. IEEE Radar Conf.*, Seattle, WA, USA, May 2017, pp. 735–738.
[31] X. Li, G. Cui, L. Kong, W. Yi, X. Yang, and J. Wu, "High speed maneuvering target detection based on joint keystone transform and CP function," in *Proc. IEEE Radar Conf.*, Cincinnati, OH, USA, May 2014, pp. 436–440.
[32] J. Zhang, T. Su, Y. Li, and J. Zheng, "Radar high-speed maneuvering target detection based on joint second-order keystone transform and modified integrated cubic phase function," *J. Appl. Remote Sens.*, vol. 10, no. 3, p. 035009, 2016.
[33] P. Huang, X.-G. Xia, G. Liao, and Z. Yang, "Ground moving target imaging based on keystone transform and coherently integrated CPF with a single-channel SAR," *IEEE J. Sel. Topics Appl. Earth Observ. Remote Sens.*, vol. 10, no. 12, pp. 5686–5694, Dec. 2017.
[34] X. Li, G. Cui, W. Yi, and L. Kong, "Fast coherent integration for maneuvering target with high-order range migration via TRT-SKT-LVD," *IEEE Trans. Aerosp. Electron. Syst.*, vol. 52, no. 6, pp. 2803–2814, Dec. 2016.
[35] X. Li, G. Cui, W. Yi, and L. Kong, "Radar maneuvering target detection and motion parameter estimation based on TRT-SGRFT," *Signal Process.*, vol. 133, pp. 107–116, Apr. 2016.
[36] M. Z. Ikram, K. Abed-Meraim, and Y. Hua, "Fast discrete quadratic phase transform for estimating the parameters of chirp signals," in *Proc. Conf. Signals, Syst. Comput.*, Pacific Grove, CA, USA, Nov. 1996, pp. 798–802.
[37] M. Z. Ikram, K. Abed-Meraim, and Y. Hua, "Fast quadratic phase transform for estimating the parameters of multicomponent chirp signals," *Digit. Signal Process.*, vol. 7, no. 2, pp. 127–135, Apr. 1997.
[38] P. Duhamel and H. Hollmann, "'Split radix' FFT algorithm," *Electron. Lett.*, vol. 20, no. 1, pp. 14–16, Jan. 1984.
[39] J. Zhang, T. Su, J. Zheng, and X. He, "Novel fast coherent detection algorithm for radar maneuvering target with jerk motion," *IEEE J. Sel. Topics Appl. Earth Observ. Remote Sens.*, vol. 10, no. 5, pp. 1792–1803, May 2017.
[40] X. Li, L. Kong, G. Cui, and W. Yi, "A low complexity coherent integration method for maneuvering target detection," *Digit. Signal Process.*, vol. 49, pp. 137–147, Feb. 2016.
[41] X.-G. Xia, "Discrete chirp-Fourier transform and its application to chirp rate estimation," *IEEE Trans. Signal Process.*, vol. 48, no. 11, pp. 3122–3133, Nov. 2000.
[42] Y. Wei and G. Bi, "Fast algorithms for polynomial time frequency transform," *Signal Process.*, vol. 87, no. 5, pp. 789–798, May 2007.
[43] J. Yu, J. Xu, J. Tang, and Y.-N. Peng, "An improved keystone-transform based method for long-time coherent integration of radar target," *Radar Sci. Technol.*, (in Chinese), vol. 6, no. 6, pp. 454–458, Dec. 2008.
[44] H. Yong-Bin, G. Mei-Guo, W. Jun-Ling, and Q. Guo-Jie, "The suppression and elimination of half blind velocity effect associated with keystone transform," *J. Electron. Inf.Technol.*, (in Chinese), vol. 36, no. 1, pp. 175–180, Jan. 2014.
[45] X. Huang, L. Zhang, S. Li, and Y. Zhao, "Radar high speed small target detection based on keystone transform and linear canonical transform," *Digit. Signal Process.*, vol. 82, pp. 203–215, Nov. 2018.
[46] J. Misiurewicz, K. S. Kulpa, Z. Czekala, and T. A. Filipek, "Radar detection of helicopters with application of CLEAN method," *IEEE Trans. Aerosp. Electron. Syst.*, vol. 48, no. 4, pp. 3525–3537, Oct. 2012.

**XIANG HUANG** was born in Henan, China. He received the B.S. degree from Zhengzhou University, Zhengzhou, China, in 2014. He is currently pursuing the Ph.D. degree with the National Laboratory of Radar Signal Processing, Xidian University, Xi'an, China. His research interests include radar target detection, time–frequency analysis, and inverse synthetic aperture radar signal processing.

**SHIYANG TANG** (M'16) was born in Jiangsu, China. He received the B.S. and Ph.D. degrees in electrical engineering from Xidian University, Xi'an, China, in 2011 and 2016, respectively, where he is currently a Lecturer with the National Laboratory of Radar Signal Processing. His research interests include imaging of synthetic aperture radar with curved path, and high-speed moving target detection and imaging.

**LINRANG ZHANG** was born in Shaanxi, China, in 1966. He received the M.S. and Ph.D. degrees in electrical engineering from Xidian University, China, in 1991 and 1999, respectively. He is currently a Full Professor with the National Laboratory of Radar Signal Processing, Xidian University. He has authored or co-authored three books and published over 100 papers. His research interests include radar system analysis and simulation, radar signal processing, and jamming suppression.

**SHENGYUAN LI** received the B.S. and Ph.D. degrees in electrical engineering from Xidian University, Xi'an, China, in 2013 and 2018, respectively. He is currently with the China Academy of Space Technology. His research interests include multi-in multi-out radar signal processing and high-speed moving target detection.